HAL
open science

Growing dynamical length, scaling and heterogeneities in the 3d Edwards-Anderson model

Ludovic D. C. Jaubert, Claudio Chamon, Leticia Cugliandolo, Marco Picco

To cite this version:

Ludovic D. C. Jaubert, Claudio Chamon, Leticia Cugliandolo, Marco Picco. Growing dynamical length, scaling and heterogeneities in the 3d Edwards-Anderson model. Journal of Statistical Mechanics: Theory and Experiment, 2007, 2007 (05), pp.P05001. 10.1088/1742-5468/2007/05/P05001 . hal-00123153

HAL Id: hal-00123153

https://hal.science/hal-00123153v1

Submitted on 27 Mar 2020

HAL is a multi-disciplinary open access archive for the deposit and dissemination of scientific research documents, whether they are published or not. The documents may come from teaching and research institutions in France or abroad, or from public or private research centers.

L'archive ouverte pluridisciplinaire **HAL**, est destinée au dépôt et à la diffusion de documents scientifiques de niveau recherche, publiés ou non, émanant des établissements d'enseignement et de recherche français ou étrangers, des laboratoires publics ou privés.

arXiv:cond-mat/0701116v2 [cond-mat.dis-nn] 26 Mar 2007

Growing dynamical length, scaling and heterogeneities in the 3D Edwards-Anderson model

Ludovic D. C. Jaubert[1,2], Claudio Chamon[3], Leticia F. Cugliandolo[2] and Marco Picco[2]

[1] Laboratoire de Physique, Ecole Normale Supérieure de Lyon, France
[2] Université Pierre et Marie Curie – Paris VI, Laboratoire de Physique Théorique et Hautes Energies, Jussieu, France
[3] Physics Department, Boston University, USA

Abstract. We study numerically spatio-temporal fluctuations during the out-of-equilibrium relaxation of the three-dimensional Edwards-Anderson model. We focus on two issues. (1) The evolution of a growing dynamical length scale in the glassy phase of the model, and the consequent collapse of the distribution of local coarse-grained correlations measured at different pairs of times on a single function using *two* scaling parameters, the value of the global correlation at the measuring times and the ratio of the coarse graining length to the dynamical length scale (in the thermodynamic limit). (2) The 'triangular' relation between coarse-grained local correlations at three pairs of times taken from the ordered instants $t_3 \leq t_2 \leq t_1$. Property (1) is consistent with the conjecture that the development of time-reparametrization invariance asymptotically is responsible for the main dynamic fluctuations in aging glassy systems as well as with other mechanisms proposed in the literature. Property (2), we stress, is a much stronger test of the relevance of the time-reparametrization invariance scenario.

1. Introduction

Studies of structural glasses have provided mounting evidence, both from numerical simulations [1]-[9] and experimental probes [10]-[15], that there is a growing length scale as a glass former is supercooled and the dynamics is heterogeneous across the system, with cooperative particle rearrangements occurring at the nanometer scale. More recent analysis in the glassy phase also suggests the existence of a growing length-scale and a heterogeneous character of the dynamics [16]-[25]. These findings reinforce the need to investigate the spatio-temporal fluctuations of glassy systems as a possible route to better understand the origin of the dramatic dynamical slow down in the glassy phase.

The same two characteristics, a growing dynamical length scale and spatial heterogeneities, also occur in the possibly better understood spin glass problem. Indeed, while a precise and unambiguous connection between problems with quenched disorder and structural glasses is still lacking, the possibility that such connection exists has been put forward dating back to the work by Kirkpatrick, Thirumalai and Wolynes [26]-[28],

who argued for a connection between structural fragile glasses and the p-spin disordered model. More recently, Tarzia and Moore [29] argued that, in the presence of a uniform field, the Edwards-Anderson model, even in one dimension, shares many features with the structural glass problem, such as an apparent Kauzmann temperature and a Vogel-Fulcher relaxation law. Hence, understanding the spatio-temporal fluctuations in the Edwards-Anderson model, in addition to being interesting in itself, may help elucidate similar issues in structural glasses if either a connection indeed exists between these problems, or heterogeneous dynamics is universal in glasses even though the mechanism for the slow relaxation may differ in those two systems.

In magnetic systems, aging can be globally quantified by the two-time spin-spin correlations, summed over all sites in the system. One of the consequences of heterogeneous dynamics in spin glasses is that aging, a manifestation of the breakdown of time translation invariance, should be non-uniform across the system. The random and quenched nature of the interactions naturally introduces in these cases a different dynamics from site to site [30]-[32]. In connection to the structural glass problem one is, though, interested in quantifying fluctuations that are not dictated by the random interactions but that is inherent to the glassy dynamics. Such kind of local dynamics and, in particular, local aging [32] can be described by the two-time spin-spin correlations, which instead of being spatially averaged over the whole bulk volume, are only averaged over a coarse-graining cell with volume $V_r = \ell^3$ centered at some site r:

$$C_r(t, t_w) = \frac{1}{\ell^3} \sum_{i \in V_r} s_i(t) s_i(t_w) \ . \tag{1}$$

The values of such local correlations vary spatially, and can be interpreted as representing local and spatially heterogeneous ages of the dynamical evolution of the system. In this paper we focus on the statistical properties of these two-time functions. First, we confirm that their spatial fluctuations around the average serve to define a growing correlation length in the aging regime. Second, we study the fixed temperature probability distribution function (pdf) $\rho(C_r; t, t_w, \ell, L)$ for a given pair of times t, t_w and a given coarse-graining length ℓ. L is the linear size of the system. Third, we analyse the triangular relations between the local coarse-grained two-time functions (1) measured at three pairs of times. Let us summarize these studies below before developing them in detail in the main text.

We improve the analysis of the pdfs of local correlations presented elsewhere [32, 33, 24] by taking into account the fact that the correlation length, and the coarse-graining linear length, are *finite* in simulations and presumably also in experiments. We show that, indeed, the pdfs of local correlators at different pairs of times t, t_w can be scaled onto universal curves as long as the global correlation is the same, *and* the ratio of the coarse graining length over the dynamical correlation length is held fixed. Such scaling can be understood as follows: at fixed temperature the pdf $\rho(C_r; t, t_w, \ell, L)$ depends on four parameters, two times t, t_w and two lenghts ℓ, L. The dependence on t and t_w can be replaced by a dependence on $C(t, t_w)$ and $\xi(t, t_w)$ with the former being the global correlation and the latter the correlation length evaluated at the measuring times.

This passage is exact. The global correlation is monotonic on the two times and the correlation length, as we show in Sect. 4.2, is a growing function of t_w and a decreasing function of C thus allowing for the invertion $(t, t_w) \to (C, \xi)$. The second step is a scaling assumption: that the pdfs depend on the coarse graining length ℓ, the total size L, and the scale ξ only through the ratios ℓ/ξ and ξ/L. This last step, we should stress, is really a scaling assumption, and not a trivial requirement from dimensional analysis, as the lengths ℓ, L and ξ are already dimensionless as they are measured in units of the lattice spacing. The end result is that the pdfs characterizing the heterogeneous constant temperature aging of the system can be written as

$$\rho[C_r; C(t, t_w), \ell/\xi(t, t_w), \xi(t, t_w)/L] \ , \tag{2}$$

We test this proposal numerically in the $3d$ Edwards-Anderson (EA) spin glass assuming that the thermodynamic limit applies so that the last scaling ratio disappears. It is noteworthy that a reasonable scaling with the global correlation held fixed and ignoring the correlation length dependence has been already achieved, *approximately*, in the $3d$EA model [32], as well as in kinetically constrained models [33] and Lennard-Jones systems [24]. Our finding that one has to hold the ratio ℓ/ξ constant for a full collapse, as shown here for the $3d$EA model, should also be applied in these last two cases. In the random manifold problem one studied the fluctuations of the global two-time roughness of a finite elastic line (finite L) thus reducing the two parameters, ℓ/ξ and L/ξ, to the same one [35]. The importance of having to take into account the growing correlation length in the scaling analysis of the dynamics of super-cooled liquids was stressed by Berthier [9].

Next, we analyse the relation between local correlations measured at three pairs of times (t_3, t_2), (t_2, t_1) and (t_3, t_1) on the same spatial point. We argue that the comparison between the local triangular relation and the global one can be used as a very stringent test of the time-reparametrization invariance scenario for the origin of dynamic fluctuations in glassy dynamics [32, 33].

The paper is organized as follows. In Sect. 2 we present the definition of the $3d$EA model. Section 3 recalls the main properties of the decay of the global correlation function. We discuss here several scaling forms proposed in the literature and we adopt the one that gives the best description of the data in the numerical time-window. We also recall the parametric construction relating the values of the global correlations at three different pairs of times that we shall use later in the local context. In Sect. 4 we discuss the statistics of the local coarse-grained two-time correlation functions. We analyse the two-time dependent growing correlation length and we present its most convenient representation as a function of t_w and the value of the global correlation. We study the pdf of local coarse-grained correlations and their dependence on the coarse-graining length ℓ and times t and t_w. We analyse the triangular relations between local coarse-grained correlations and we explain why the time-reparametrization invariance scenario makes a very concrete prediction for their behaviour. Finally, in Sect. 5 we present our conclusions.

2. The model

We focused on the three-dimensional Edwards-Anderson ($3d$EA) spin-glass model defined by the energy

$$H = \sum_{\langle ij \rangle} J_{ij} s_i s_j \ . \tag{3}$$

The interaction strengths J_{ij} act on nearest neighbours on a cubic $3d$ lattice and are independent identically distributed random variables taken from a Gaussian probability distribution with zero mean and unit variance. The spins s_i with $i = 1, \ldots, N = L^3$ are bimodal Ising variables. The static critical temperature is $T_g \sim 0.92$ [36].

We simulated an instantaneous quench from infinite temperature by choosing a random initial condition $s_i(0) = \pm 1$ with probability a half. We used Monte Carlo dynamics with the Metropolis algorithm to mimic the temporal relaxation of the spin-glass coupled to an external environment at temperature T. A Monte Carlo step (MCs) corresponds to N randomly chosen spin flip attempts.

We used lattices with linear size $L = 60$ and $L = 100$ and, in order to reduce finite size effects, we set periodic boundary conditions in all directions. We present simulations at $T = 0.6$; this value is optimal in the sense that it is not too close to the critical point and critical fluctuations should be thus reduced, and it is not too low so that the dynamics is not prohibitively sluggish. Similar results are obtained for a bimodal distribution of coupling strengths. For the time-scales reached, finite size effects are not important, as we checked by varying the system sizes.

3. Global self-correlation

The two-time *self-correlation*

$$C(t, t_w) = N^{-1} \sum_{i=1}^{N} s_i(t) s_i(t_w) \tag{4}$$

measures the overlap of the spin configurations at times t_w, the waiting-time, and t, the measuring time. It characterizes the *global* or *macroscopic* non-equilibrium relaxation of glassy systems. In the large N limit and for long but finite times, that is to say well before equilibration, the self-correlation (4) is self-averaging with respect to noise and disorder induced fluctuations [37]. By using then a few samples we reach longer time scales ($\sim 10^8$ MCs) for similar system sizes than previously done in the literature.

The two-time dependence of (4) is well-understood in coarsening systems [38] away from criticality where two two-time regimes are simply ascribed to equilibrium thermal fluctuations within the ordered domains and non-equilibrium domain-wall motion. In the limit $t \geq t_w \gg t_0$, with t_0 some microscopic time scale, the correlation can be written as a sum of two terms representing these two-time regimes:

$$C(t, t_w) = C_{st}(t - t_w) + C_{ag}(t, t_w) \tag{5}$$

with the limit conditions

$$C_{st}(0) = 1 - q_{ea} \ , \qquad \lim_{t_w \to t^-} C_{ag}(t, t_w) = q_{ea} \ ,$$
$$\lim_{t - t_w \to \infty} C_{st}(t - t_w) = 0 \ , \qquad \lim_{t \gg t_w} C_{ag}(t, t_w) = 0 \ .$$

q_{ea} is a measure of the equilibrium ordering. A finite limit of the equilibrium – stationary – part of the correlation, C_{st}, is a *sine qua non* condition for the existence of a finite temperature phase transition.

In ferromagnets and p spin disordered models the non-equilibrium term C_{ag} satisfies dynamic scaling,

$$C_{ag}(t, t_w) \sim q_{ea} \ f\left(\frac{R(T,t)}{R(T,t_w)}\right) \ , \tag{6}$$

with $R(T,t)$ a monotonic function of time. The label $_{ag}$ indicates the aging character of the dynamics in the sense that older systems (longer t_w's) have a slower decay than younger ones (shorter t_w's). Dynamic scaling (6) implies that any three correlations between three generic times $t_0 \ll t_3 < t_2 < t_1$ and taking values below the plateau at q_{ea} are related by

$$C_{ag}(t_1, t_3) = q_{ea} \ f\left\{f^{-1}[C_{ag}(t_1, t_2)/q_{ea}] \ f^{-1}[C_{ag}(t_2, t_3)/q_{ea}]\right\} \ , \tag{7}$$

independently of the functional form of $R(T,t)$.

In the Sherrington-Kirkpatrick (SK) model [40] the aging part of the correlation has itself a hierarchical organisation and satisfies dynamic ultrametricity

$$C_{ag}(t_1, t_3) = \min[C_{ag}(t_1, t_2), C_{ag}(t_2, t_3)] \tag{8}$$

for generic times $t_1 > t_2 > t_3 \gg t_0$ such that all correlations take values below the plateau at q_{ea}. The asymptotic character of this result makes it difficult to be observed in a numeric simulation. A preasymptotic scaling

$$C_{ag}(t, t_w) \sim q_{ea} \ f\left(\frac{R(T_c, t - t_w)}{R(T_c, t_w)}\right) \ , \qquad \text{with} \qquad R(T_c, t) \sim \ln t/t_0 \ . \tag{9}$$

that reaches the ultrametric relation (8) in the long times limit was found in the trap model at its critical temperature [41].

Several numerical studies of the self-correlation (4) in the $3d$EA model appeared in the literature [42]-[47]. The first difficulty encountered is the identification of a plateau separating equilibrium and out-of-equilibrium relaxations. This separation is not as clear as desired in the numerical data that could as well be described with a scaling that is compatible with the absence of a finite temperature phase transition – a multiplicative scaling as found for instance in problems of elastic lines in low dimensional random environments [35, 48]. However, evidence for a finite temperature phase transition in the $3d$EA model [49] suggests the additive scaling (5). Experiments on an insulating spin-glass sample are consistent with this type of scaling too [50].

The existence of a special value of C at q_{ea} as well as the behaviour of the data below this value can be examined by constructing parametric plots of the correlations and thus testing the relations (7) and (8). In Fig. 1 we plot $C(t_1, t_2)$ against $C(t_2, t_3)$ at $T = 0.6$, using three pairs of t_3, t_1 (given in the caption) that yield different values of

$C(t_1, t_3)$. The construction shows a rather clear change in regime when $C(t_1, t_2)$ passes through the value ~ 0.78 and when $C(t_2, t_3)$ reaches the same value. One can interpret the change from rather straight and flat behaviour (vertical or horizontal) to the curved piece in-between as a change in the two-time scaling that operates when each of the correlations goes beyond q_{ea}. (Note that the vertical behaviour when t_2 gets close to t_1 is neater than the horizontal behaviour when t_2 gets close to the opposite limit t_3; this is a finite time effect, the two-time scale separation improves at longer times.) The straight line pieces indicate an ultrametric relation between correlation values lying above the breaking point and correlation values lying below it. This is consistent with an additive separation between a stationary regime and an aging one.

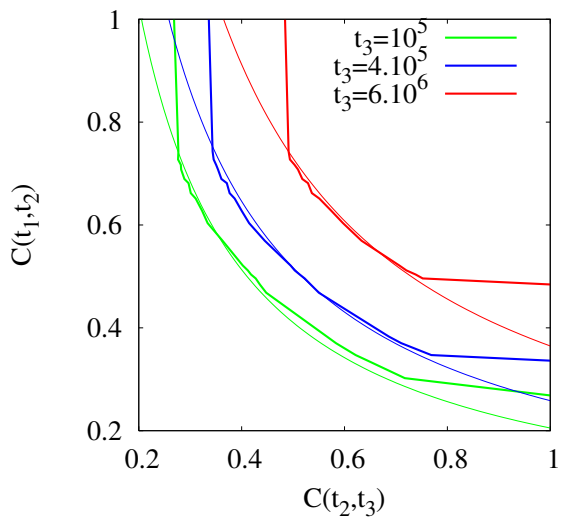

Figure 1. Parametric plot of the correlation functions $C(t_1, t_2)$ against $C(t_2, t_3)$ using t_2 as a parameter varying between t_3 and t_1. The curves are averaged over 5 or 7 samples. We use $t_1 = 1.3 \times 10^8$ MCs and three values of t_3 (given in the key) that lead to three values of $C(t_1, t_3)$. As a guide-to-the-eye we show with thin solid lines the hyperbolic functions $q_{ea}\ C(t_1, t_3)/C(t_2, t_3)$ that fit the data correctly in the curved parts of the plot.

The curved pieces (correlations taking values below the breaking points that we identify with q_{ea}) is very far from a double straight line with a square angle as expected for a full dynamic ultrametric behaviour. It is instead rather well described by a hyperbolic function with parameter $q_{ea} \sim 0.78$. The data are not in the trully asymptotic regime and before discarding the dynamic ultrametric behaviour one should test the relevance of its preasymptotic form (9).

In the ideal asymptotic limit of very long-waiting time and very long time-difference the contribution of the stationary part should saturate to zero and the full correlation to a constant q_{ea}. However, the approach to the constant can be rather slow – it is a power in mean-field models – and thus interfere in the aging regime. One then subtracts the stationary contribution, assumed to be a power law,

$$C_{st}(t - t_w) \sim A(t - t_w)^{-\alpha} \tag{10}$$

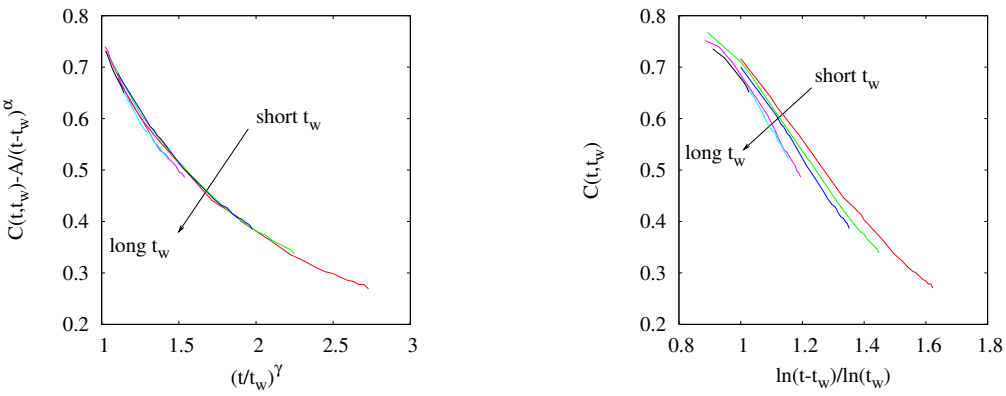

Figure 2. Test of two two-time regimes with simple aging (a), and ultrametric scaling (b). The waiting-times are $t_w = 10^5,\ 4\times10^5,\ 10^6,\ 6\times10^6,\ 10^7$ and $t_w = 5\times10^7$ MCs. $A = 10\pm2$ and $\alpha = 0.5\pm0.05$ and $\gamma = 0.14$.

with A and α two fitting parameters [51]. A more refined analysis, including a waiting-time dependent correction to the stationary part estimated along the lines of the droplet picture, appeared in [45]. In Fig. 2 we compare the scaling form (6) with $R \sim t^\gamma$, called 'simple aging' [51] and the pre-asymptotic ultrametric scaling (9). The drift with increasing waiting-time is shown with an arrow. It is clear that, even though the collapse is not perfect, the simple aging form yields a much better description of the data. We checked that other functions, $R(T,t)$, such as the logarithmic growth of the droplet model are not as good.

In conclusion, even though the numerical data are not utterly conclusive, they support the existence of a plateau at a finite q_{ea}, with a rather slow approach of the stationary part to it, and an aging contribution that is best described by a simple aging form, $R(t) \sim t^\gamma$ with $\gamma \sim 0.14$. The values of the other parameters are $q_{ea} \sim 0.8$, $A = 10$ and $\alpha \sim 0.5$; the function $f(x)$ is then very close to $f(x) \sim q_{ea}/x$. In short,

$$C_{st}(t-t_w) \sim 10\ (t-t_w)^{-0.5}\ , \qquad C_{ag} \sim 0.8\left(\frac{t_w}{t}\right)^{0.14}\ . \tag{11}$$

Note that this form is totally different from the analytic solution to the SK model [40], the mean-field version of the $3d$EA model. We shall use the triangular construction in Sect. 4.4 to analyse dynamic fluctuations.

4. Local fluctuations

The local coarse-grained correlation is defined similarly to the global one [32]

$$C_r(t,t_w) = N_r^{-1}\sum_{i=1}^{N_r} s_i(t)s_i(t_w) \tag{12}$$

where the sum runs over the $N_r = \ell^3$ spins lying in a cubic box with linear size ℓ centered at the site r. We work with overlapping coarse-graining boxes centered on each site of

the lattice. In this way we improve the statistics obtaining N data points *per* sample. It is important to notice that working with Ising spins we have a natural discretization of the local correlations: C_r varies between -1 and 1 in steps of $2/\ell^3$. This effect is negligible when $\ell > 6$ in such a way that $2/\ell^3 < 0.01$ but it is annoying for smaller values, *e.g.* $\ell = 3,\ 4$. Averaging over short time-windows does not change significantly our results.

The simplest way to investigate local fluctuations is to study the probability density function $\rho(C_r)$. This function depends on five parameters: the two times t and t_w, the coarse-graining length ℓ, the linear size of the system L, and the temperature T that, in particular, determines the Edwards-Anderson order parameter q_{ea}. In this paper we keep temperature fixed and henceforth ignore the temperature dependence. We use sufficiently large systems sizes so that in practice $L \to \infty$.

A more refined analysis of the fluctuations that puts the global time-reparametrization invariance scenario to the test consists in comparing local correlations measured at three pairs of times and studying the behaviour of local triangular relations.

4.1. Evolution of the pdf with the measuring time t

We start by analysing the evolution of ρ with the value of its mean, or global self-correlation, C, obtained using $t_w = 5 \times 10^4$ MCs and the corresponding t's (given in the caption) at fixed and rather small coarse-graining length, $\ell = 3$. The curves in Fig. 3 (a) show that for all C values there is a peak at $C_r \sim 0.85$ that is slightly higher than the value of q_{ea} estimated from the study of the global self-correlation. The height of the peak diminishes with decreasing C while the weight on the tail on negative C_r's increases. Using such a small coarse-graining volume, many boxes partially reverse when times are sufficiently separated. Two undesired effects of using coarse-graining volumes that are too small are thus clearly identified and can be easily interpreted within a domain-growth picture of two competing equilibrium states. At long waiting-times a patchwork of domains with relatively large radii establishes. The density of domain walls is small. Using a small coarse-graining volume one has a high probability of contouring a region that remains in the 'basin of attraction of the equilibrium state' in which it is at time t_w, with no domain-walls crossing the box – independently of how many of these states exist. In these cases, the local coarse-grained correlation is reduced from one just by thermal fluctuations and should then be very close to q_{ea} (if the size of the coarse-graining box is really small one can imagine that not even all the thermal fluctuations needed to reach q_{ea} enter the box and thus the peak can be at a higher value). When time passes, more and more of these boxes are crossed or traversed by domain walls and the weight of the peak diminishes while the tail of the pdf increases. In a simple coarsening picture with only two equilibrium states that develop relatively rapidly and thin domain walls between them, one should see a second peak developing at $-q_{ea}$ due to regions that have reversed, from one equilibrium state to the other, after the passage of a domain-wall (or an odd number of them). For the values of the global

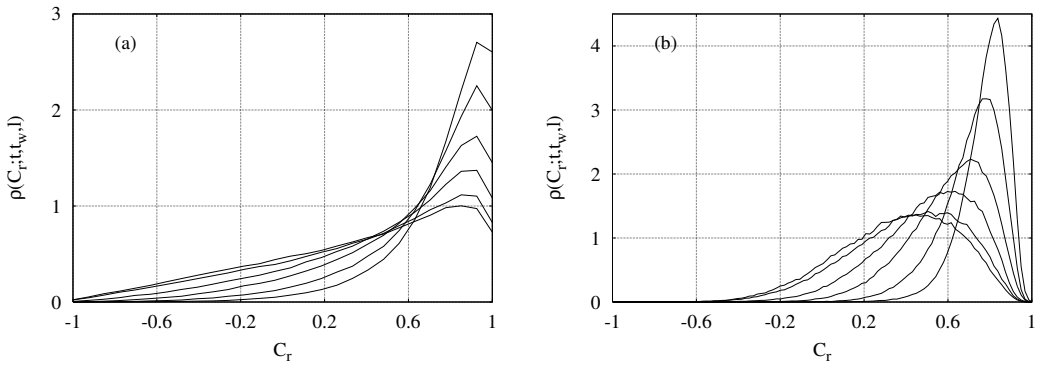

Figure 3. Dependence of the pdf of local coarse-grained correlations on the value of the global correlation at fixed t_w and varying t. The waiting time is fixed to $t_w = 5\times10^4$ MCs. The total times are $t = 6.5\times10^4$ MCs ($C = 0.78$), $t = 1.2\times10^5$ MCs ($C = 0.7$), $t = 3\times10^5$ MCs ($C = 0.6$), $t = 10^6$ MCs ($C = 0.5$), $t = 5.5\times10^6$ MCs ($C = 0.4$), and $t = 9\times10^6$ MCs ($C = 0.36$), and leads to the global correlation values given between parenthesis. Coarse-graining box with linear size $\ell = 3$ (a) and $\ell = 6$ (b). The height of the peak diminishes and stays located at the same C in (a) while it drifts to the left in (b). The left tail grows with increasing t in both cases.

correlation (total times) reached we do not see this process here.

The stationary character of the peak at $C_r \sim q_{ea}$ is lost using a larger coarse-graining box, as shown in Fig. 3 (b). This panel also shows the evolution with t of the pdf of local correlations at fixed $\ell = 6$. When $t = t_w$ the pdf is just a delta function at one. As t departs from t_w one enters the stationary regime and the pdf is approximately Gaussian around its mean value $C > q_{ea}$. Upon further increasing t one enters the interesting aging regime and the pdf departs from being Gaussian, it develops a tail towards small values of C_r and its skewness becomes negative. At sufficiently long t the pdf starts symmetrizing and the fluctuations eventually become Gaussian again when the average C reaches zero.

Finally, in Fig. 4 we show the dependence of the pdf of local coarse-grained correlations on the size of the coarse-graining box measured at a fixed pair of times t and t_w such that the global correlation is $C = 0.5$. The distribution evolves from a rather wide negatively skewed form, with the peak at $C_r \sim q_{ea}$ and an important tail on negative C_r's to a Gaussian pdf centered at C upon increasing ℓ. In the limit $\ell = L$, the linear size of the system, the distribution concentrates on the global value C. The figure shows data for ℓ varying from 3 to 20.

It is clear from the analysis above that one needs to use a sufficiently large coarse-graining box to avoid finite size and discretization effects. To study non-Gaussian statistics, too large coarse-graining boxes should be equally avoided. In the next Section we analyse the correlation length and we then give a concrete criterion to achieve the scaling regime.

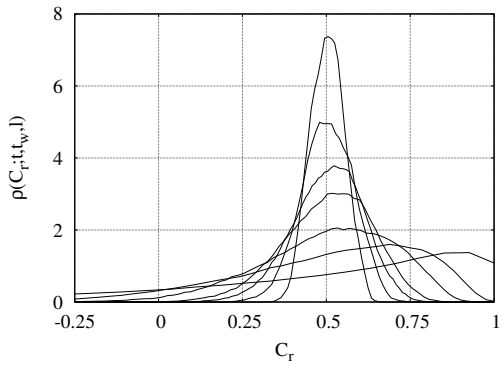

Figure 4. Dependence of the pdf of local coarse-grained correlations on the size of the coarse-graining box for fixed total time, t, and waiting-time, t_w; $t_w = 5 \times 10^4$ MCs and $t = 10^6$ MCs in such a way that the global correlation is $C = 0.5$ for all data sets. The coarse-graining lengths are $\ell = 3$, 5, 7, 10, 12, 15, 20 and as ℓ increases the pdfs get narrower and their maximum moves towards smaller C.

4.2. The correlation length

As in usual ordering processes one would like to identify a correlation length and determine its temperature and time-dependence. A *two-time* correlation length, $\xi(t, t_w)$, apt to describe the growth of order in the low-temperature aging regime, can also be defined from the study of a two-site two-time correlation. In the spin language one defines [32]

$$C_4(r; t, t_w) = N^{-1} \sum_{i,j=1}^{N} \left[\left(s_i(t) s_i(t_w) s_j(t) s_j(t_w) - C^2(t, t_w) \right] \right._{|\vec{r}_i - \vec{r}_j| = r} \tag{13}$$

and extracts ξ from the fits of its decay as a function of r to an exponential. The results of this analysis are shown in Fig. 5 (a) where we plot $\xi(t, t_w)$ as a function of $t - t_w$ for three values of t_w given in the caption. A better representation of the same data is given in Fig. 5 (b) where we display ξ as a function of $1 - C$, evaluated at the same times. The curves are now monotonic in both $1 - C$ and t_w. Finally, the t_w-dependence can be taken into account by proposing, see Fig. 5 (c),

$$\xi(t, t_w) \sim \begin{cases} \xi_{st}(t - t_w) & \text{for } C > q_{ea} \ , \\ t_w^a \ g(C) & \text{for } C < q_{ea} \ , \end{cases} \tag{14}$$

with $a \sim 0.065$ and $g(C)$ a monotonically decreasing function of C.

We can also extract the two-time dependence of a typical length scale, to be associated to the correlation length, from the analysis of the functional form of the pdf of local coarse-grained correlations. If the pdfs of coarse-grained correlations are close to a Gaussian, one has summed over uncorrelated variables and the coarse-graining linear length has gone beyond the correlation length (at the working times t and t_w). On the other hand, a pdf that differs from a Gaussian should be due to correlations in the underlying variables (see the discussion in [33]).

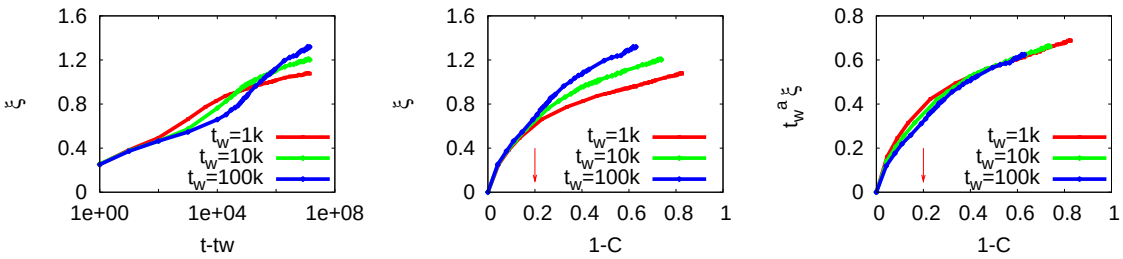

Figure 5. Study of the two-time dependent correlation length as extracted from the spatial decay of C_4 ion a $3d$EA model with $L = 100$. (a) As a function of time-delay. (b) As a funtion of the global correlation. (c) Power law scaling with the waiting-time.

For instance one can analyse the evolution of the skewness $S \equiv \langle (C_r - \langle C_r \rangle)^3 \rangle / \langle (C_r - \langle C_r \rangle)^2 \rangle^{3/2}$ and deduce the generic trend of ξ by choosing a reference value S^* to determine the coarse-graining length at which Gaussian statistics is approached. In this way we obtain $\xi(t_w, C)$ with the same characteristics as the one shown in Fig. 5.

In [32] one found $\xi(t, t_w) \sim (tt_w)^a$ with a a small exponent or else a logarithmic law of the product of the two times. We here prefer to use the more precise description in eq. (14). Note that the maximum value of the correlation length reached is just a few lattice spacings, also consistent with the results found in the studies using the two-replica analysis [46, 47].

Finally, let us point out a sharp difference between our results for the dynamical correlation length in the glassy phase of the $3d$EA model and those found in supercooled liquids. In the latter, studies of the correlation between the order parameter fluctuations measured at different times t and t_w on different regions of a single evolving sample found a non-monotonic behavior as a function of $\Delta t = t - t_w$ [3, 15, 62] (there is no waiting-time dependence there since the system is in a metastable state with equilibrium-like dynamics). More specifically, the integral over space of the four point correlation $\chi_4(\Delta t) \equiv \int d^d r \; C_4(r, \Delta t)$ increases with *Deltat* until reaching a maximum at a temperature-dependent Δt^* where it starts falling-off towards zero. The value of Δt^* and the maximum $\chi_4^* \equiv \chi_4(\Delta t^*)$ increase when approaching the glass transition, and mode-coupling theories predict their divergence as a power law of the distance from criticality, $T - T_{mct}$ at the mode-coupling transition [57]. In our case, we work not above but, instead, below the glass transition temperature of the $3d$EA model, and the strictly increasing correlation length is accompanied by a monotonically increasing $\chi_4(t - t_w, t_w)$ as a function of $t - t_w$, for fixed t_w.

4.3. Time-scaling

We are interested in characterizing $\rho(C_r; t, t_w, \ell, L)$ in the thermodynamic limit taken at the outset ($L \to \infty$), and in the asymptotic limit taken with a prescription that we now explain. Exploiting once again the monotonic character of the two-time global

correlation, the probability density becomes $\rho(C_r; C, t_w, \ell)$ where we keep the name ρ to simplify the notation. Now, we would like to take the limit $t_w \to \infty$ while keeping C fixed – to any value below the plateau q_{ea} – but we need to specify whether we keep ℓ finite or we let it go to infinity together with t_w to obtain an interesting asymptotic limit. The arguments in [32, 33, 58] and the analysis of the numerical results discussed in Sect. 4.2 suggest that $\xi(t, t_w)$ diverges in the limit $t_w \to \infty$ and/or $t \to \infty$. Thus, if we keep ℓ fixed while we let $t_w \to \infty$ we are effectively taking smaller and smaller boxes with respect to the correlation length ξ and thus considering regions that are artificially more and more correlated. This effect can be seen by plotting the pdf of local coarse-grained correlations at fixed C obtained by using different pairs t and t_w and a fixed ℓ: there is a slow drift of the weight of the pdf towards the peak at q_{ea}. In Fig. 6 (a) we display the pdf of local correlations C_r for several values of the pair of times t and t_w that lead to the same global value $C = 0.6$. The coarse-graining length is $\ell = 5$ in all cases. The curves do indeed show a slow drift for increasing t_w with the peak moving towards higher values of C_r and an increasing weight of the tail on negative values.

We are then forced to take larger and larger coarse-graining sizes as t_w and t increase to attain a stable asymptotic limit of the probability distributions. The divergence of ℓ should follow the one of ξ – that is relatively slow. Considering diverging coarse-graining boxes one should also get rid of the C_r's that are close to and above q_{ea} or negative. Of course, reaching this limit in a numerical simulation is impossible and one is forced to deal with finite times and finite coarse-graining size effects.

The qualitative discussion above can be made quantitative by exploiting the monotonic character of ξ with t and C. We can actually rewrite the pdf as a function of the global correlation and the correlation length, $\rho(C_r; C, \xi, \ell)$. Using now a natural scaling assumption in which lengths ξ and ℓ enter only through their ratio, then $\rho(C_r; C, \ell/\xi)$. As in standard critical phenomena universal behaviour should then appear in the limit:

$$\lim_{\substack{(t,t_w,\ell)\to\infty \\ C(t,t_w)=C \\ \ell/\xi\to 0}} \rho(C_r; t, t_w, \ell) = \rho(C_r, C) \ . \tag{15}$$

The limit $\ell/\xi \to 0$ is impossible to impose in a numerical simulation since the values of the correlation length are relatively small ($\xi < 10$). In practice, we shall then avoid this limit and simply work with the requirement ℓ/ξ fixed to achieve a good data collapse. A rough estimate of the growth of the coarse-graining length needed to scale the data is then given as follows. The global correlation in the aging regime scales as t/t_w, approximately (see the analysis in Sect. 3). In order to keep C constant one approximately multiplies the two times t and t_w by the same constant, say ν. Under the simultaneous dilation of times the correlation length transforms as

$$\xi(\nu t, \nu t_w) \sim (\nu t_w)^a \, g(C) = \nu^a \, \xi(t, t_w) \tag{16}$$

where, for simplicity, we adopted the power-law behaviour [see Sect. 4.2 for the analysis

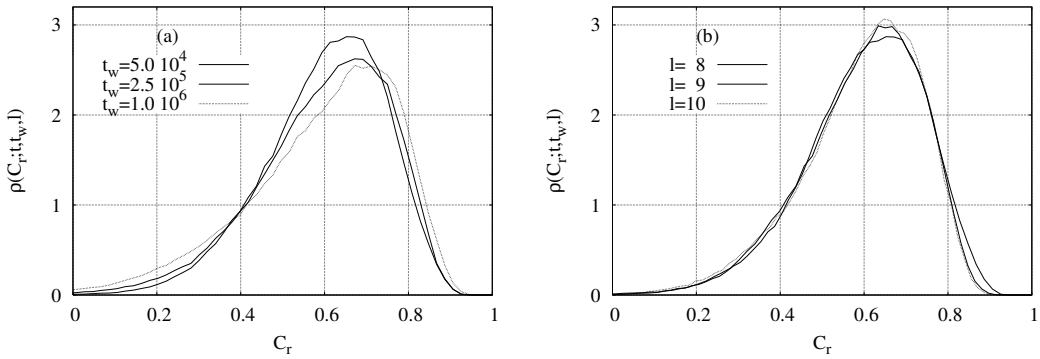

Figure 6. Pdf of local correlations C_r. (a) C_r is coarse-grained on boxes of linear size $\ell = 8$ at $C = 0.6$ fixed. The curves correspond to three waiting-times given in the key. There is a slow drift with increasing t_w (see the text). (b) C_r is coarse-grained on boxes with variable length ℓ. The global correlation is the same as in panel (a), $C = 0.6$. The curves correspond to $t_w = 5 \times 10^4$ and $\ell = 8$, $t_w = 2.5 \times 10^5$ and $\ell = 9$, and $t_w = 10^6$ and $\ell = 10$. The collapse is improved with respect to panel (a).

of $\xi(t, t_w)$]. We then estimate the change in coarse-graining length as

$$\ell(\nu t, \nu t_w) \sim \nu^a \ell(t, t_w) \ . \tag{17}$$

Given that the exponent a is very small, $a \sim 0.1$, the change in ℓ is also quite small. For instance, if $\nu = 2$, the scaling factor is $\nu^a \sim 1.14$.

In Fig. 6 (b) we take into account the increasing correlation length with times t and t_w and we then use a variable coarse-graining length to study the data at the same pairs of times. The values of ℓ chosen follow the estimate (17) – though they slightly differ from it – and are given in the key. With the variable coarse-graining one manages to locate the maxima at the same position. The collapse between the two longer waiting-times is now very good while the shorter waiting-time still has too much weight on large values of C_r and a lower weight on the peak than expected. We believe that this is due to finite-time effects. Note also that in the ideal theoretical limit one should have no weight at all above $q_{ea} \sim 0.8$ which is certainly not the case in the numerical data. The crossover between stationary and aging regimes is contaminating our data, especially at short waiting-times. Unfortunately, we have reached the limit of our numerical time-window and we cannot present results for older systems.

The analysis of numerical data in other glassy systems should also take into account the growth of the correlation lenght. In particular, the approximate but not excellent collapse of the pdfs of local incoherent correlation functions in Lennard-Jones mixtures [24] should be corrected by taking into account the need to use a variable coarse-graining length [61].

4.4. Triangular relations

The global time-reparametrization invariance [32] suggests that in the ideal asymptotic limit the slow part of the coarse-grained *local* correlations should scale as

$$C_{ag}(r;t,t_w) \approx q_{ea}\ f\left(\frac{h(r,t)}{h(r,t_w)}\right)\ , \tag{18}$$

with f the *same* function describing the global correlation [eq. (6)] in the ideal limit $1 \ll \ell \ll \xi$ [32]. The sum rule $C_{ag}(t,t_w) = V^{-1}\int d^d r\ C_{ag}(r;t,t_w)$ applies. We now present some tests of eq. (18) that are based on the parametric representation of the dynamics.

In Sect. 3 we showed that two-time functions with a separation of time-scales as in eq. (5) and an aging scaling as in eq. (11) are related in a parametric way in which times disappear. Equation (18) implies that the local (fluctuating) two-time functions should verify the *same* relation

$$C_{ag}(r;t_1,t_3) = q_{ea}\ f\left\{f^{-1}[C_{ag}(r;t_1,t_2)/q_{ea}]\ f^{-1}[C_{ag}(r;t_2,t_3)/q_{ea}]\right\}\ . \tag{19}$$

This is a result of the fact that time-reparametrization invariance restricts the fluctuations to appear only in the local functions $h(r,t)$ while the function f is locked to be the global one everywhere in the sample.

A pictorial inspection of this relation should take into account the fact that while the stationary decay is not expected to fluctuate, the full aging relaxation and, in particular, the minimal value of the local two-time functions, $C(r;t_1,t_3)$, are indeed fluctuating quantities. The parametric construction on different spatial regions should yield 'parallel translated' curves with respect to the global one, as displayed in Fig. 1. Fluctuations in the function f would yield different functional forms in the curved part of the parametric construction. A more quantitative analysis can be done by using the knowledge of f that can be extracted from the global correlation decay. Indeed, if f is known, the parametric plot $f^{-1}(C_{r12}/q_{ea})/\sqrt{f^{-1}(C_{r13}/q_{ea})}$ against $f^{-1}(C_{r23}/q_{ea})/\sqrt{f^{-1}(C_{r13}/q_{ea})}$ should yield a master curve identical to the global one with different sites just being advanced or retarded with respect to the global value. This is another way of stating that the sample ages in a heterogeneous manner, with some regions being younger (other older) than the global average. [For simplicity we used a short-hand notation, $C_{r\mu\nu} = C(r;t_\mu,t_\nu)$ with $\mu,\nu = 1,2,3$.] If the time-reparametrization mode is indeed flat the local values should lie all along this master curve in the aging regime.

The conclusions drawn above apply in the strict $1 \ll \ell \ll \xi$ limit. In simulations and experiments ξ is finite and even rather short. Thus, ℓ is forced to also be a rather small parameter, in which case 'finite size' fluctuations in f are also expected to exist. The claim is that the latter should scale down to zero faster (in ℓ) than the fluctuations that are related to the zero mode.

We have tested these claims in the non-equilibrium dynamics of the $3d$ EA spin-glass. The results are shown in Fig. 7. In the upper left panel we show the global triangular relation (thick black line) as well as the local one on four chosen sites.

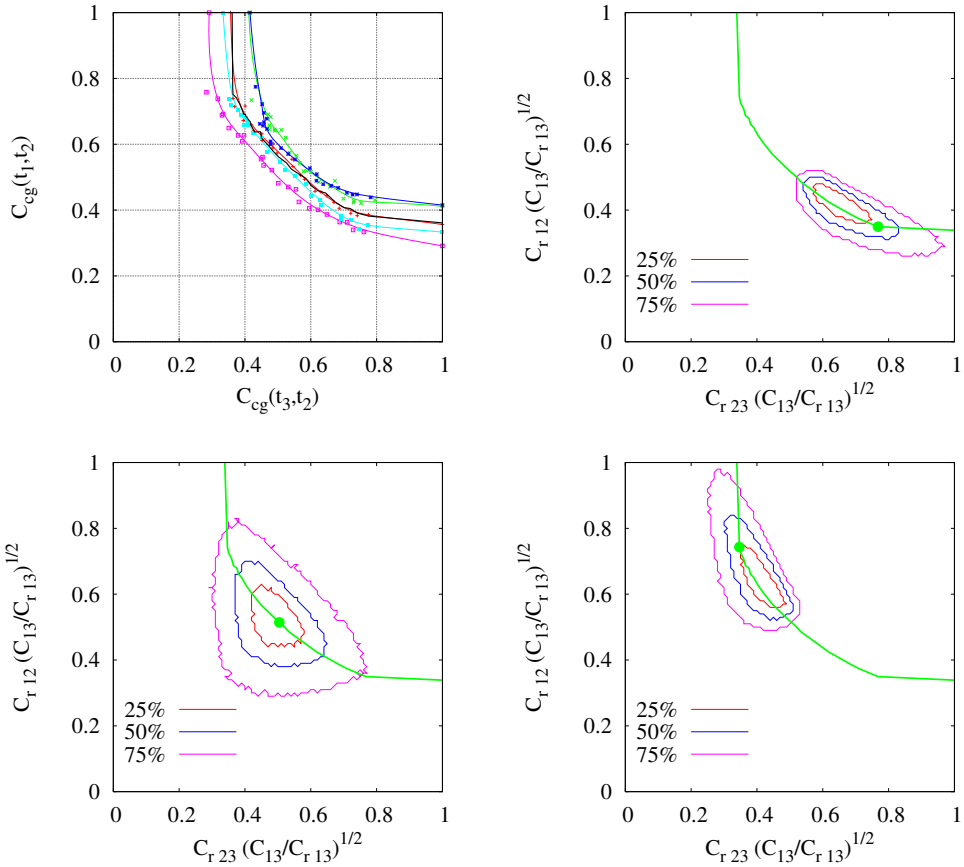

Figure 7. The triangular relation in the $3d$EA model with $L = 100$. Upper left panel: the thick (black) line represents the global $C(t_1, t_2)$ against $C(t_2, t_3)$ using t_2 as a parameter varying between $t_3 = 5 \times 10^4$ MCs and $t_1 = 9 \times 10^6$ MCs, $C(t_1, t_3) \sim 0.35$ and $q_{ea} \sim 0.8$, *cfr.* Fig. 1. With different points joined with thin lines we show the triangular relations between the local coarse-grained correlations on five randomly chosen sites on the lattice ($\ell = 30$). Upper right panel and lower left and right panels: $2d$ projection of the joint probability density of $C(r; t_1, t_2)\sqrt{C(t_1, t_3)/C(r; t_1, t_3)}$ and $C(r; t_2, t_3)\sqrt{C(t_1, t_3)/C(r; t_1, t_3)}$ at fixed three values of the intermediate time, $t_2 = 1.5 \times 10^5$ MCs, 8×10^5 MCs and 5×10^6 MCs, respectively and $\ell = 10$. The global $C(t_1, t_2)$ against $C(t_2, t_3)$ using t_2 as a parameter is shown with a thick green line. The green points indicate the location of $C(t_1, t_2)$ and $C(t_2, t_3)$ for the chosen t_2's. Each point in the scatter plot corresponds to a site, r. The lines indicate the boundary surrounding 25%, 50% and 75% of the probability density. The cloud extends mostly along the global relation as predicted by time-reparametrization invariance.

The separation of time-scales is clear in the plot. The local curves are quite parallel indeed. In the remaining panels in Fig. 7 we show the $2d$ projection of the joint probability density (using contours that encircle 25%, 50%, and 75% of the probability) of the site fluctuations in the local coarse-grained correlations at different chosen times $t_2 = 1.5 \times 10^5$ MCs (upper right), $t_2 = 8 \times 10^5$ MCs (lower left), and $t_2 = 5 \times 10^6$ MCs (lower right). Taking advantage of the fact that $f(x) \sim x^{-1}$ we use a very convenient normalization in which we multiply the horizontal and vertical axes by $\sqrt{C_{13}/C_{r13}}$.

Global time-reparametrization invariance, expressed in eq. (19), implies that the data points should spread *along* the global curve indicated with a thick green line in the figure. Some sites could be advanced, others retarded, with respect to the global value – shown with a point on the green curve – but all should lie mainly on the same master curve. This is indeed quite well reproduced by the simulation data in the three cases, $C(t_1, t_2)$ close to $C(t_1, t_3)$ (upper right panel), $C(t_1, t_2)$ close to q_{ea} (lower right panel), and $C(t_1, t_2)$ far from both (lower left panel). Most of the data points tend to follow the master curve though some fall away from it. The reason for this is that eq. (19) should be strictly satisfied only in the very large coarse-graining volume limit ($\ell \gg 1$) with $\ell/\xi \ll 1$ while we are here using $\ell = 10 \gtrsim \xi$, see the discussion in Sect. 4.2.

Finally, notice that, in contrast to the growing correlation length scale, there is no blatantly obvious explanation of these triangular relations within other theoretical scenarios. These relations are perhaps the most direct consequence of the time reparametrization symmetry arguments.

4.5. Normal form of the pdfs

Once we established that, due to the growth of the correlation length, it is necessary to use different coarse-graining lengths to compare the pdf of local correlations evaluated at different times we now go back to the raw data and we study the functional form of the pdfs, *cfr.* Fig. 3. The reason for this study is that the time-reparametrization invariance scenario yields precise predictions on the functional form that one would like to test [33].

To this end, we change variables and we plot $\sigma\rho(C_r)$ against $(C_r - C)/\sigma$ with σ the mean-square displacement. Note that, due to the scaling hypothesis σ also depends on C and ℓ/ξ. Evidently, the transformation into the normal form is not sufficient to eliminate the dependence on C and ℓ/ξ from ρ. Keeping this fact in mind, we present data for $\sigma\rho(C_r) > 10^{-3}$ in Fig. 8.

Several features of these curves deserve a careful description. First, the abrupt end of the data on the right is due to the finite values of ℓ. Indeed, the probability is strictly zero for $C_r > 1$ while it is notably different from zero for $C_r = 1$ as soon as ℓ is finite and not too large. Second, for small values of ℓ the peak is located close to q_{ea} while it moves to the left for increasing ℓ. Third, it is clear that the decay on the right of the peak is much faster than the one on the left. Fourth, for small ℓ the dependence on C appears on the tails (left and right) and it disappears close to the peak, *cfr.* Fig. 3.

One can now try to find a convenient functional form to describe the numerical data for sufficiently large ℓ, say of the order of $\xi(t, t_w) \sim 5$. In [33] the pdfs of the local connected correlations in kinetically facilitated models and the global spin-spin correlation (4) in small size $3d$EA models for values of C that are not too far from q_{ea} were analysed using an extension of the Gumbel distribution of extreme value statistics:

$$\Phi_a(y) = \frac{|\alpha| a^a}{\Gamma(a)} \, \mathrm{e}^{a\left(\alpha(y-y_0) - \mathrm{e}^{\alpha(y-y_0)}\right)} \,, \tag{20}$$

where $\Gamma(a)$ is the *gamma* function. The parameters y_0 and α control the position of the center and the width of the distribution, respectively. By fixing the parameters $\alpha = \sqrt{\Psi'(a)}$ and $y_0 = [\log a - \Psi(a)]/\alpha$ where $\Psi(a)$ is the *digamma* function $\Psi(a) = \Gamma'(a)/\Gamma(a)$, one ensures that the center is at zero and the width is unity. The Gumbel distribution with with *integer* parameter $a \geq 1$ describe the distribution of the a-th largest (smallest) value in a sequence of independent identically distributed random variables with a probability density decaying faster than any power law. For any a, there is a choice of sign for α and the two signs correspond to the Gumbel statistics of either extreme minima or extreme maxima. If the Gumbel is taken to its normal form by fixing the coefficient α, it approaches the normal form of the Gaussian for increasing a.

In Fig. 8 we compare the numerical data to the functional form (20) and the Gaussian with zero mean and unit variance. The data on each panel are for three values of the global correlation $C \sim 0.7$, $C \sim 0.6$ and $C \sim 0.5$ not too far from $q_{ea} \sim 0.8$; the difference between panels is the length of the coarse-graining box, $\ell = 5$ (a), $\ell = 10$ (b), $\ell = 15$ (c). For small ℓ the complete data deviate from both functional forms. There is, as expected, a systematic dependence on C that is most clear on the left tail. An exponential decay of the tail on the left (as found in the Gumbel form) yields a satisfactory description of the data for each C at sufficiently small $(C_r - C)/\sigma$, as shown by the straight line. As ℓ increases the data get closer to (20) on the whole range – note however that the numerical data are constrained to vary between $(-1 - C)/\sigma$ and $(1 - C)/\sigma$ on the horizontal axis (shown with vertical arrows) while the independent variable in the functional form (20) can take any real value. In panels (b) and (c) there is no systematic dependence on C. The value of the parameter a has been chosen to yield the best description of the full set of data, finding that a increases with increasing ℓ thus approaching a Gaussian (though it has not reached it yet for $\ell = 15$).

In summary, for *finite* ξ one identifies three functional forms of the pdf of local correlations, once put in normal form:

- $\ell \ll \xi$ Nothing special (since for small ξ this means ℓ of the order of the lattice spacing).
- $\ell \sim \xi$ Gumbel-like.
- $\ell \gg \xi$ Gaussian.

Note that in the ideal t, $t_w \to \infty$, and $\xi \to \infty$ limits one should have an interesting scaling regime when $\ell/\xi \to 0$, now with ℓ very large.

Let us focus on sufficiently long coarse-graining lengths such that the Gumbel and then Gaussian functional forms give a reasonable description of the data with a variable a. The full pdf and hence the parameter a itself depend on the two times and the coarse-graining length ℓ. Trading the two times by the global correlation and the correlation length, as explained in Sect. 4, one has $a(t, t_w, \ell) \to a(C, \xi, \ell)$. One again, our scaling hypothesis implies $a(C, \ell/\xi)$. Quite remarkably, the pdfs once presented in normal form, and in particular a, do not show a strong dependence on C in the accessed range of

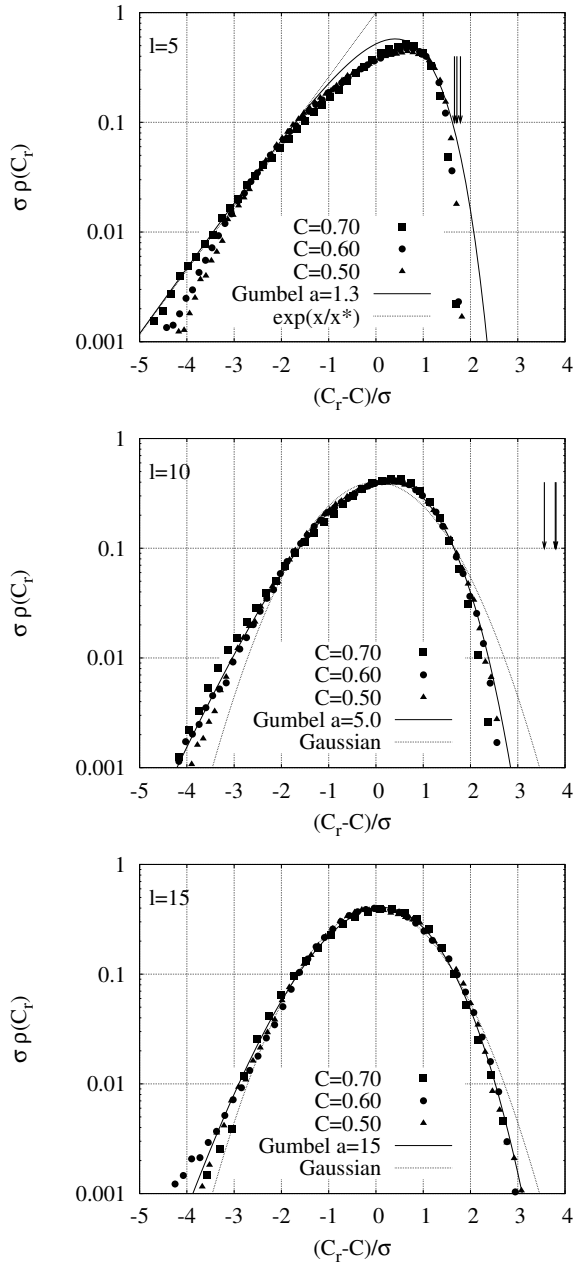

Figure 8. Normal form of the pdf of local coarse-grained correlations at $t_w = 5 \times 10^4$ and $t = 1.2 \times 10^5$ ($C = 0.701$), $t = 3 \times 10^5$ ($C = 0.601$) and $t = 10^6$ ($C = 0.503$) and different values of the coarse-graining length $\ell = 5,\ 10,\ 15$ as indicated in the keys. Comparison to different functional forms, in particular the Gumbel (solid line) and the Gaussian (dashed line) functions. The three arrows indicate the right-edge of the numerical distribution, $(1 - C)/\sigma$. The values of σ are the following. When the global correlation is $C = 0.701$: $\sigma = 0.180$ for $\ell = 5$, $\sigma = 0.0785$ for $\ell = 10$ and $\sigma = 0.0455$ for $\ell = 15$. When the global correlation is $C = 0.601$: $\sigma = 0.233$ for $\ell = 5$, $\sigma = 0.112$ for $\ell = 10$ and $\sigma = 0.0675$ for $\ell = 15$. When the global correlation is $C = 0.503$: $\sigma = 0.278$ for $\ell = 5$, $\sigma = 0.131$ for $\ell = 10$ and $\sigma = 0.0772$ for $\ell = 15$. Note that the exponential fit of the left tail gives a quite correct description for $C = 0.701$ and $\ell = 5$ but for larger values of ℓ the tail deviates since the pdf is approaching the Gaussian.

values.

Recently, Bertin and Clusel gave a simple explanation of the ubiquity of Gumbel-like probability distributions of fluctuations [60]. They showed that sums of infinitely many correlated random variables, with special correlations, are distributed according to a Gumbel functional form. In the case in which the correlation arises due to a rewriting of the maximum of a sequence as a sum over ordered differences, one finds the ordinary Gumbel pdf of extreme value statistics. For other, more general correlations one finds that the sum is distributed according to the Gumbel functional form with a continuous parameter a (even other functions are possible). In our problem, the local coarse-grained correlations are, by construction, sums of correlated random variables. The fact that we find a functional form that resembles a generalized Gumbel distribution, with a parameter that depends on ℓ and the value of the global correlation, is then consistent with the observation of Bertin and Clusel.

From our point of view, these results are interesting and support the conjecture that the development of global time-reparametrization invariance is the mechanism by which dynamic fluctuations generate in glassy dynamics. Indeed, the phenomenological effective action for local fluctuations proposed in [33] suggested by this symmetry captures this functional form when $C \lesssim q_{ea}$.

5. Conclusions

The peculiar dynamics of glassy systems, leading to an asymptotically divergent correlation length, implies that highly non-trivial fluctuations will still be present at longer and longer length scales as times increase. Local fluctuations can be captured by studying coarse-grained local two-time correlations, which provide a measure of local aging in the system, while the global measure of aging is obtained by simply taking the coarse-graining length to be the bulk system size L. The presence of a growing length scale affects the distributions of local correlations, in that larger and larger regions in space become correlated, and the local average over a coarse-graining region will not be simply Gaussian-distributed if the coarse-graining length ℓ is not much larger than the two-time correlation length $\xi(t, t_w)$.

In this paper we studied the effect of such growing length scale on the scaling of the distributions of local correlations in the $3d$EA model. We found that the pdfs of local coarse-grained correlations $\rho(C_r; t, t_w, \ell, L)$ can be scaled into universal curves that depend on the four parameters t, t_w, ℓ, L only through three scaling variables: the value of the global correlation $C(t, t_w)$, and the ratios between the length scales and the correlation length, $\ell/\xi(t, t_w)$ and $\xi(t, t_w)/L$. (As we stressed in the paper, the lengths ℓ, L and ξ are already dimensionless as they are measured in units of the lattice spacing, and hence the scaling as a function of the correlation length is a scaling assumption, and does not follow from trivial dimensionless analysis.) The influence of a 'measuring' length, in this case the total length, was also stressed in the study of roughness fluctuations of elastic manifolds [35].

Because the shape of the pdfs of local correlations depend on the correlation length and the coarse-graining length, one can use the form of the pdfs to extract the growing length scale. The values of the correlation length so obtained are comparable to those acquired directly from four-point correlation functions. Morever, we analysed the evolution of the functional form of the pdf of local correlations with the coarse-graining length ℓ. By comparing to a Gumbel-like functional form we studied the dependence of its characterising parameter, a, with the coarse-graining volume and we linked these observations to recent generic results on sums of correlated random variables [60].

The universal scalings for the pdfs of local correlations for the $3d$EA model should be applicable to other glassy systems as well, if there is universality in glassy behavior among systems that share common features such as aging behavior and a growing dynamical length scale. Indeed, progress in this direction has been already made in [24], where the pdfs for local correlations in the glassy phase of Lennard-Jones binary mixtures were shown to *approximately* collapse when grouped by fixing the value of the global correlation and in [33] where kinetically constrained lattice models were analysed. According to our findings the collapse in structural glasses should become even sharper if the coarse graining box sizes are scaled so as to account for the growing dynamical length scale. A similar phenomena, though stationary in time and with a length-scale controlled by the distance from 'criticality' in temperature, are expected to appear in super-cooled liquids too [9].

The existence of a growing correlation length can be explained within the time-reparametrization invariance scenario [63] but it could also be associated to other theoretical proposals such as theories based on the mode-coupling approach or random first order scenario [57] and its refinement including the effect of entropic droplets [64], dynamical criticality controlled by a zero-temperature critical point [65] and frustration limited domains [66], at least in the super-cooled liquid. We then presented an analysis of the local coarse-grained correlations that constitutes, to our understanding, a much more stringent test of the time-reparametrization invariance scenario. This consists in comparing the local and global triangular relations for correlations measured at three times. Our results are consistent with the concrete predictions of the time-reparametrization invariance approach. Together with the tests of the local fluctuation-dissipation deviations [32] these are the most accurate tests of the time-reparametrization invariant theory.

Acknowledgements

LFC is a member of Institut Universitaire de France. We thank H. Castillo, G. Fabricius, T. Grigera, J. L. Iguain, H. Makse, D. Stariolo and L. Valluzzi for very useful

discussions. We wish to especially thank L. Berthier, S. Franz and an anonymous referee for their very useful comments on the contents and presentation of our results, and C. Aron for assistance in the preparation of the figures. LFC thanks the Newton Institute at the University of Cambridge, UK, and the Universidad Nacional de Mar del Plata, Argentina, and LDCJ the LPTHE at the Université Pierre et Marie Curie – Paris VI, France, for hospitality during the preparation of this work. This work is supported in part by the NSF Grants DMR-0305482 and DMR-0403997 (CC).

[1] B. B. Laird and H. R. Schober, Phys. Rev. Lett. **66**, 636 (1991); H. R. Schober and B. B. Laird, Phys. Rev. B **44**, 6746 (1991).
[2] T. Muranaka and Y. Hiwatari, Phys. Rev. E **51**, R2735 (1995); M. M. Hurley and P. Harrowell, Phys. Rev. E **52**, 1694 (1995); D. N. Perera and P. Harrowell, Phys. Rev. E **59**, 5721 (1999).
[3] N. Lacevic, F. W. Starr, T. B. Schrder, V. N. Novikov, and S. C. Glotzer, Phys. Rev. E **66**, 030101(R) (2002) and references therein.
[4] A. Heuer and A. Okun, J. Chem. Phys. **106**, 6176 (1997); B. Doliwa and A. Heuer, Phys. Rev. Lett. **80**, 4915 (1998).
[5] G. Johnson, A. I. Mel'cuk, H. Gould, W. Klein, and R. D. Mountain, Phys. Rev. E **57**, 5707 (1998).
[6] R. Yamamoto and A. Onuki, Phys. Rev. E **58**, 3515 (1998).
[7] F. W. Starr, S. Sastry, J. F. Douglas, and S. C. Glotzer, Phys. Rev. Lett. **89**, 125501 (2002).
[8] C. Oglichler and H. R. Schober, Phys. Rev. B **59**, 811 (1999).
[9] L. Berthier, Phys. Rev. E **69**, 020201(R) (2004).
[10] H. Sillescu, J. Non-Crystal. Solids **243**, 81 (1999). M. D. Ediger, Annu. Rev. Phys. Chem. **51**, 99 (2000).
[11] E. Weeks, J. C. Crocker, A. C. Levitt, A. Schofield, and D. A. Weitz, Science **287**, 627 (2000).
[12] E. R. Weeks and D. A. Weitz, Phys. Rev. Lett. **89**, 095704 (2002).
[13] E. Vidal Russell, N. E. Israeloff, L. E. Walther, and H. Alvarez Gomariz, Phys. Rev. Lett. **81**, 1461 (1998); L. E. Walther, N. E. Israeloff, E. Vidal Russell, and H. Alvarez Gomariz, Phys. Rev. B **57**, R15112 (1998); E. Vidal Russel and N. E. Israeloff, Nature **408**, 695 (2000).
[14] R. S. Miller and R. A. MacPhail, J. Phys. Chem. **101**, 8635 (1997).
[15] L. Berthier, G. Biroli, J-P Bouchaud, L. Cipelletti, D. El Masri, D. L'Hôte, F. Ladieu, M. Pierno, Science **310**, 1797 (2005).
[16] K. Vollmayr-Lee, W. Kob, K. Binder, and A. Zippelius, J. Chem. Phys. **116**, 5158 (2002).
[17] L. Buisson, L. Bellon, and S. Ciliberto, cond-mat/0210490, to appear in Proceedings of "III Workshop on Non-Equilibrium Phenomena" (Pisa 2002).
[18] W. K. Kegel and A. V. Blaaderen, Science **287**, 290 (2000).
[19] K. S. Sinnathamby, H. Oukris, N. E. Israeloff, Phys. Rev. Lett. **95**, 67205 (2005). Crider and N. E. Israeloff, Nano Letters **6**, 887 (2006).
[20] L. Cipelletti, H. Bissig, V. Trappe, P. Ballestat, and S. Mazoyer, J. Phys.: Condens. Matter **15**, S257 (2003); A. Duri and L. Cipeletti, cond-mat/0606051
[21] R. E. Courtland and E. R. Weeks, J. Phys.: Condens. Matter **15**, S359 (2003). G. C. Cianci, R. E. Courtland, E. R. Weeks, cond-mat/0512698. E. R. Weeks, J. C. Crocker, D. A. Weitz, cond-mat/0610195.
[22] P. Wang, C. Song, and H. A. Makse, Nature Physics 2, - pp526 - 531 (2006); cond-mat/0611033.
[23] G. Parisi, J. Phys. Chem. B **103**, 4128 (1999).
[24] H. E. Castillo and A. Parsaeian, cond-mat/0610857.
[25] A. Parsaeian and H. E. Castillo, cond-mat/0610789.

[26] T. R. Kirkpatrick and D. Thirumalai, Phys. Rev. B **36**, 5388 (1987); Phys. Rev. B **37**, 5342 (1988); Phys. Rev. A **37**, 4439 (1988); J. Phys. A **22**, L149(1989); D. Thirumalai and T. R. Kirkpatrick, Phys. Rev. B **38**, 4881 (1988).
[27] T. R. Kirkpatrick and P. Wolynes, Phys. Rev. A **35**, 3072 (1987). T. R. Kirkpatrick and P. Wolynes, Phys. Rev. B **36**, 8552 (1987).
[28] T. R. Kirkpatrick, D. Thirumalai, P. G. Wolynes, Phys. Rev. A **40**, 1045 (1989).
[29] M. Tarzia and M. A. Moore, cond-mat/0609113.
[30] F. Romá, S. Bustingorry, P. M. Gleiser, D. Dominguez, cond-mat/0608603.
[31] S. C. Glotzer, N. Jan, T. Lookman, A. B. MacIsaac, and P. H. Poole, Phys. Rev. E **57**, 7350 (1998). A. Barrat and R. Zecchina, Phys. Rev. E **59**, R1299 (1999). F. Ricci-Tersenghi and R. Zecchina, Phys. Rev. E **62**, R7567 (2000). A. Montanari and F. Ricci-Tersenghi, Phys. Rev. Lett. **90**, 017203 (2003), Phys. Rev. B **68**, 224429 (2003).
[32] H. E. Castillo, C. Chamon, L. F. Cugliandolo, and M. P. Kennett, Phys. Rev. Lett. **88**, 237201 (2002). H. E. Castillo, C. Chamon, L. F. Cugliandolo, J. L. Iguain, and M. P. Kennet, Phys. Rev. B **68**, 134442 (2003).
[33] C. Chamon, P. Charbonneau, L. F. Cugliandolo, D. R. Reichman, and M. Sellitto, J. Chem. Phys. **121**, 10120 (2004).
[34] C. Chamon, L. F. Cugliandolo, and H. Yoshino, J. Stat. Mech (2006) P01006.
[35] S. Bustingorry, J. L. Iguain, C. Chamon, L. F. Cugliandolo, and D. Domínguez, cond-mat/0603503.
[36] M. Pleilimg and I. A. Campbell, Phys. Rev. B **72**, 184429 (2005).
[37] See L. F. Cugliandolo, *Dynamics of glassy systems*, cond-mat/0210312 for a review.
[38] A. Bray, Adv. in Phys. **43**, 357 (1994).
[39] L. F. Cugliandolo and J. Kurchan, Phys. Rev. Lett. **71**, 173 (1993).
[40] L. F. Cugliandolo and J. Kurchan, J. Phys. A **27**, 5749-5772 (1994).
[41] E. Bertin and J.-P. Bouchaud, J. Phys. A **35**, 3039-3051 (2002).
[42] J. O. Anderson, J. Mattson, and P. Svedlindh, Phys. Rev. B **46**, 8297 (1992).
[43] H. Rieger, J. Phys. A **26**, L615 (1993).
[44] M. Picco, F. Ricci-Tersenghi, F. Ritort, Eur. Phys. J. B **21**, 211 (2001).
[45] T. Komori, H. Takayama, and H. Yoshino, J. Phys. Soc. Jpn. **68**, 3387 (1999), *ibid* **69**, 1192 (1999), **69** Suppl. A 228 (2000).
[46] J. Kisker, L. Santen, M. Schrenckenberg, and H. Rieger, Phys. Rev. B **53**, 6418 (1996).
[47] L. Berthier and J.-P. Bouchaud, Phys. Rev. B **66**, 054404 (2002).
[48] H. Yoshino, J. Phys. A **29**, 1421 (1996); Phys. Rev. Lett. **81**, 1493 (1998); and unpublished. A. Barrat, Phys. Rev. E **55**, 5651 (1997).
[49] E. Marinari, G. Parisi, and J. J. Ruiz-Lorenzo, Phys. Rev. B **58**, 14852 (1998). M. Pallassini and S. Caracciolo, Phys. Rev. Lett. **82**, 5128 (1999).
[50] D. Hérisson and M. Ocio, Phys. Rev. Lett. **88**, 257202 (2002); Eur. Phys. J. B **40**, 283 (2004).
[51] E. Vincent, J. Hammann, M. Ocio, J-P. Bouchaud, and L. F. Cugliandolo cond-mat/9607224.
[52] D. A. Huse, Phys. Rev. B **43**, 8673 (1991).
[53] E. Marinari, G. Parisi, F. Ricci-Tersenghi, and J. J. Ruiz-Lorenzo, J. Phys. A **33**, 2373 (2000).
[54] H. Yoshino, K. Hukushima, and H. Takayama, Phys. Rev. B **66**, 064431 (2002).
[55] K. Hukushima, H. Yoshino, H. Takayama, Prog. Theor. Phys. Supp. **138**, 568 (2000). V. Dupuis, E. Vincnt, J-P Bouchaud, J. Hammann, H. Aruga-Katori, A. Ito, Phys. Rev. B **64**, 174204 (2001).
[56] Y. G. Joh, R. Orbach, G. G. Wood, J. Hammann, and E. Vincent, Phys. Rev. Lett. **82**, 438 (1999)
[57] S. Franz and G. Parisi, J. Phys. C **12**, 6335 (2000). C. Donati, S. Franz, G. Parisi, and S.C. Glotzer, J. Non-Cryst. Solids **307**, 215 (2002). G. Biroli and J-P Bouchaud, Europhys. Lett. **67** (2004) 21. G. Biroli, J-P Bouchaud, K. Miyazaki, D. R. Reichman, cond-mat/0605733.
[58] C. Chamon, M. P. Kennett, H. E. Castillo, and L. F. Cugliandolo, Phys. Rev. Lett. Phys. Rev. Lett. **89**, 217201 (2002).
[59] S. T. Bramwell, P.C. W. Holdsworth, and J. F. Pinton, Nature **396**, 552 (1998).

[60] E. Bertin and M. Clusel, J. Phys. A **39**, 7607-7619 (2006).

[61] L. Valluzzi *et al* in preparation.

[62] C. Toninelli, M. Wyart, L. Berthier, G. Biroli, J-P Bouchaud Phys. Rev. E **71**, 041505 (2005).

[63] C. Chamon and L. F. Cugliandolo, *Fluctuations in glassy systems*, submitted to JSTAT special issue *Principles of dynamical systems*.

[64] T. R. Kirkpatrick and P. Wolynes, Phys. Rev. B **36**, 8552 (1987). T. R. Kirkpatrick, D. Thirumalai and P. G. Wolynes, Phys. Rev. A **40**, 1045 (1989). P. G. Wolynes, Jour. Res. NIST **102**, 187 (1997). J-P Bouchaud and G. Biroli, J. Chem. Phys. **121**, 7347 (2004).

[65] J. P. Garrahan and D. Chandler, Proc. Natl. Acad. Sci. USA **100**, 9710 (2003). S. Whitelam, L. Berthier, and J. P. Garrahan Phys. Rev. Lett. 92, 185705 (2004). A. C. Pan, J. P. Garrahan, and D. Chandler Phys. Rev. E **72**, 041106 (2005). R. L. Jack, L. Berthier, and J. P. Garrahan, Phys. Rev. E **72**, 016103 (2005). R. L. Jack and J. P. Garrahan, J. Chem. Phys. 123, 164508 (2005),

[66] G. Tarjus, S. A. Kivelson, Z. Nussinov, and P. Viot, *The frustration-based approach of supercooled liquids and the glass transition: a review and critical assessment*, cond-mat/0509127 and references therein.

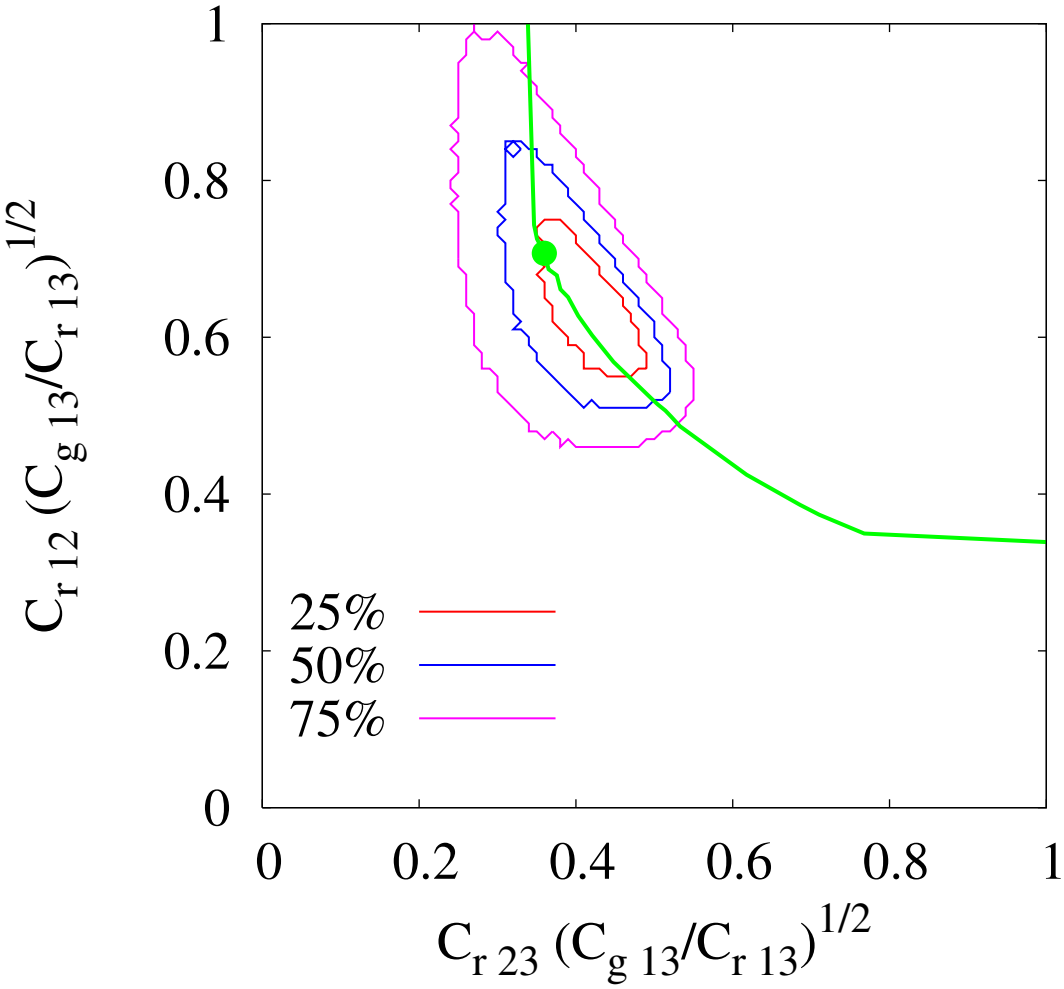
1
0.8
0.6
0.4
0.2
0
0
0.2
0.4
0.6
0.8
1
25%
50%
75%
$C_{r\,12}\,(C_{g\,13}/C_{r\,13})^{1/2}$
$C_{r\,23}\,(C_{g\,13}/C_{r\,13})^{1/2}$